

## Are Silicon Nanoparticles an Interstellar Dust Component?

Aigen Li and B.T. Draine

*Princeton University Observatory, Peyton Hall, Princeton, NJ 08544, USA;*  
agli@astro.princeton.edu, draine@astro.princeton.edu

### ABSTRACT

Silicon nanoparticles (SNPs) have been proposed as the source of the observed “extended red emission” (ERE) from interstellar dust. We calculate the thermal emission expected from such particles, both in a reflection nebula such as NGC 2023 and in the diffuse interstellar medium (ISM). Pure neutral Si SNPs would emit at  $16.4\mu\text{m}$ , while Si/SiO<sub>2</sub> SNPs (both neutral and charged) produce a feature at  $20\mu\text{m}$ . Observational upper limits on the  $16.4\mu\text{m}$  and  $20\mu\text{m}$  features in NGC 2023 impose upper limits of  $< 1.5\text{ppm}$  in pure Si SNPs, and or  $< 0.2\text{ppm}$  in Si/SiO<sub>2</sub> SNPs. The observed ERE intensity from NGC 2023 then gives a lower bound on the required photoluminescence efficiency  $\eta_{\text{PL}}$ . For foreground extinction  $A_{0.68\mu\text{m}} = 1.2$ , we find  $\eta_{\text{PL}} > 5\%$  for Si SNPs, or  $\eta_{\text{PL}} > 24\%$  for Si/SiO<sub>2</sub> SNPs in NGC 2023. Measurement of the R band extinction toward the ERE-emitting region could strengthen these lower limits. The ERE emissivity of the diffuse interstellar medium appears to require  $\gtrsim 42\%$  ( $\gtrsim 33\%$ ) of solar Si abundance in Si/SiO<sub>2</sub> (Si) SNPs. We predict IR emission spectra and show that DIRBE photometry appears to rule out such high abundances of free-flying SNPs in the diffuse ISM. If the ERE is due to SNPs, they must be either in clusters or attached to larger grains. Future observations by SIRTf will be even more sensitive to the presence of free-flying SNPs.

*Subject headings:* dust, extinction — infrared: ISM: lines and bands — reflection nebulae: NGC 2023

### 1. Introduction

First detected in the Red Rectangle (Schmidt, Cohen, & Margon 1980), “extended red emission” (ERE) from interstellar dust consists of a broad, featureless emission band between  $\sim 5400\text{Å}$  and  $9000\text{Å}$ , peaking at  $6100\text{Å} \lesssim \lambda_p \lesssim 8200\text{Å}$ , and with a width  $600\text{Å} \lesssim \text{FWHM} \lesssim 1000\text{Å}$ . The ERE has been seen in a wide variety of dusty environments: the diffuse interstellar medium (ISM) of our Galaxy, reflection nebulae, planetary nebulae, HII regions, and other galaxies (see Witt, Gordon, & Furton 1998 for a summary). The ERE is generally attributed to photoluminescence (PL) by some component of interstellar grains, powered by ultraviolet (UV)/visible photons. The photon conversion efficiency of the diffuse ISM has been determined to be near  $(10 \pm 3)\%$  (Gordon et al. 1998; Szomoru & Guhathakurta 1998) assuming that all UV/visible photons absorbed by interstellar grains are absorbed by the ERE carrier. The actual photoluminescence efficiency  $\eta_{\text{PL}}$  of the ERE carrier must exceed  $\sim 10\%$ , since the ERE carrier cannot be the only UV/visible photon absorber.

Various forms of carbonaceous materials – hydrogenated amorphous carbon (HAC) (Duley 1985; Witt &

Schild 1988), polycyclic aromatic hydrocarbons (PAHs) (d’Hendecourt et al. 1986)<sup>1</sup> quenched carbonaceous composite (QCC) (Sakata et al. 1992), C<sub>60</sub> (Webster 1993), coal (Papoular et al. 1996), PAH clusters (Allamandola, private communication), and carbon nanoparticles (Seahra & Duley 1999)<sup>2</sup> – have been proposed as carriers of ERE. However, most candidates appear to be unable to simultaneously match the observed ERE spectra and the required PL efficiency (see Witt et al. 1998 for details).

Very recently, Witt et al. (1998) and Ledoux et al. (1998) suggested crystalline silicon nanoparticles (SNPs) with 15 Å – 50 Å diameters as the carrier on the basis of experimental data showing that SNPs could provide a close match to the observed ERE spectra and satisfy the quantum efficiency requirement. It was estimated by Witt et al. (1998) and Ledoux et al. (1998) that SNPs account for  $\lesssim 5\%$  of the total interstellar dust mass, with Si/H  $\approx 6$  ppm. Zubko et al. (1999) modelled the interstellar extinction curve taking SNPs as an interstellar dust component containing Si/H  $\approx 18$  ppm, or  $\sim 50\%$  of the solar abundance  $[\text{Si}/\text{H}]_{\odot} = 36$  ppm. More recently, Smith & Witt (2001) have further developed the SNP model for the ERE, concluding that the observed ERE in the diffuse ISM can be explained with Si/H = 6 ppm in SiO<sub>2</sub>-coated SNPs with Si core radii  $a \approx 17.5$  Å.

The purpose of this paper is to test the SNP hypothesis. We calculate the IR spectra for SNPs in a reflection nebula – NGC 2023 – and compare with observations. We show that the SNPs in NGC 2023 contain Si/H  $\lesssim 1.5$  ppm. We re-estimate the *minimum* Si depletion in SNPs required to account for the observed ERE intensity in the diffuse ISM, and calculate the IR emission expected from such particles. We show that existing DIRBE photometry appears to rule out the abundances of free-flying SNPs required to account for the ERE emissivity of the diffuse ISM. Future observations by the *Space Infrared Telescope Facility* (SIRTF) will be even more sensitive to the abundance of SNPs in the diffuse ISM.

In §2 we discuss the optical properties of silicon nano-crystals and glassy SiO<sub>2</sub> (§2.1) as well as the heat capacities of pure Si and Si core-SiO<sub>2</sub> mantle grains (§2.2). In §3 we carry out calculations for the IR emission spectra of SNPs (with or without SiO<sub>2</sub> coatings), and discuss their implications. In §4 we discuss the effects of grain shape, mantle thickness, and sources of uncertainties. Our conclusions are presented in §5.

## 2. Grain Physics

Experimental studies indicate that high photoluminescence efficiencies are only observed from Si nanocrystals when their surfaces have been “passivated” by oxidation or hydrogenation – otherwise electron-hole pairs recombine nonradiatively (see, e.g., Kovalev et al. 1999). Accordingly, SNPs with oxide coatings are likely

---

<sup>1</sup>High photoluminescence efficiencies can be obtained by PAHs. Arguments against PAHs as ERE carriers include: (1) presence of sharp structures in the luminescence spectra of individual PAH molecules in contrast to the featureless nature of the interstellar ERE spectra; (2) lack of spatial correlation between the ERE and the PAH IR emission bands in the compact HII region Sh 152 (Darbon et al. 2000) and in the Orion Nebula (Perrin & Sivan 1992); (3) ERE detection in the Bubble Nebula where no PAH emission has been detected (Sivan & Perrin 1993); (4) nondetection of ERE emission in reflection nebulae illuminated by stars with effective temperatures  $T_{\star} < 7000$  K (Darbon, Perrin, & Sivan 1999) whereas PAHs emission bands have been seen in such regions (e.g., see Uchida, Sellgren, & Werner 1998) and are expected for the PAH emission model (A. Li & B.T. Draine 2001, in preparation). Argument (1) may not be fatal since a featureless band may result from a mixture of many individual PAH molecules and ions.

<sup>2</sup>Seahra & Duley (1999) argued that small carbon clusters were able to meet both the ERE profile and the PL efficiency requirements. However, this hypothesis appears to be ruled out by non-detection in NGC 7023 of the 1  $\mu\text{m}$  ERE peak (Gordon et al. 2000) predicted by the carbon nanoparticle model.

to be of primary interest as the source of the ERE. However, we will also discuss the infrared emission of pure Si SNPs in order to show that even if the Si core dominates the IR emission, the IR spectral signature is still conspicuous.

## 2.1. Optical Properties

The optical properties of crystalline Si nanoparticles are controversial. Some studies (see Yoffe 2001 for a recent review) have concluded that the optical properties of Si nanoparticles differ substantially from those of bulk Si. This has been attributed to the quantum confinement effect (Wang & Zunger 1994; Tsu, Babic, & Ioriatti 1997). Koshida et al. (1993; hereafter KKS93) have published dielectric constants for crystalline nanosilicon which are considerably smaller than those of *bulk*-Si. We find that the absorption and reflectivity measurements for porous silicon (e.g., Koshida et al. 1993, de Filippo et al. 2000) appear to be inconsistent with the KKS93 optical constants; instead, they can be approximately reproduced using a mixture of Si and voids, if the Si component is described using the optical constants of bulk Si, as previously found by Kovalev et al. (1996), Theiss (1997), Léron del, Madéore, & Muller (2000), and Diesinger, Bsiesy, & Hérino (2001). Oxide layers are generally also present in laboratory samples of porous Si; we find that the absorption and reflectance spectra can also be satisfactorily reproduced using Bruggeman effective medium theory (Bohren & Huffman 1984) for a mixture of voids, SiO<sub>2</sub>, and bulk-Si.

We take the following “synthetic” approach to obtain the complex refractive index  $m(\lambda) = m' + im''$  for bulk Si at low temperatures, with no electron-hole pairs present (the contribution of electron-hole pairs will be treated separately). For  $0.01 < \lambda < 1.2\mu\text{m}$  we take  $m''$  of Adachi (1999) for bulk crystalline Si. For  $1.2 < \lambda < 3.6\mu\text{m}$  we set  $m'' = 2.4 \times 10^{-8}$  estimated from the (room temperature) absorption coefficient  $\alpha \approx 10^{-3}\text{cm}^{-1}$  of bulk Si between 1 and  $3\mu\text{m}$  (Gray 1972). For  $3.6 < \lambda < 25\mu\text{m}$  we take those of Palik (1985) for crystalline bulk Si; extrapolation is then made for  $\lambda > 25\mu\text{m}$ .<sup>3</sup> After smoothly joining the adopted  $m''$ , we calculate  $m'$  from  $m''$  through the Kramers-Kronig relation (Bohren & Huffman 1983, p. 28).

The Si long-wavelength absorption properties will depend on whether any free electrons or holes are present. SNPs are thought to luminesce only when uncharged and containing exactly one electron-hole pair, which recombines radiatively in  $\sim 10^{-3}\text{s}$  (Smith & Witt 2001). The thermal energy remaining after luminescence will then be radiated by a SNP with no free electrons or holes, at least in the diffuse ISM where the cooling time is short compared to the time between absorption of UV photons. For these SNPs, we use the optical properties of bulk Si.

Charged SNPs will contain at least one free electron or hole, which we assume contributes to the dielectric function

$$\delta\epsilon \approx \frac{-(\omega_p\tau)^2}{(\omega_p\tau)^2 + i\omega\tau} \quad (1)$$

$$\omega_p^2 = \frac{3|Z|}{4\pi a_{\text{Si}}^3} \frac{e^2}{4\pi m_{\text{eff}}} \quad (2)$$

---

<sup>3</sup>We do not adopt those of Palik (1985) for  $\lambda > 25\mu\text{m}$  since they were measured at  $T \approx 300\text{K}$ , and the  $\lambda > 25\mu\text{m}$  absorption is dominated by thermally-excited electron-hole pairs. In the absence of such pairs, we approximate  $m''(\lambda) \approx m''(25\mu\text{m})(25\mu\text{m}/\lambda)$ . The IR bands of Si nanoparticles may become stronger due to the symmetry-breaking surfaces (e.g., see Hofmeister, Rosen, & Speck 2000). New IR bands, forbidden in bulk Si, may also appear (Adachi, private communication). Unfortunately, IR measurements of Si nanoparticles are unavailable, so we must use the optical properties of bulk Si.

where we adopt an effective mass  $m_{\text{eff}} \approx 0.2m_e$  for electrons or holes in Si.<sup>4</sup> Scattering by the Si boundary will result in  $\tau \approx a/v_F$ , where we take  $v_F \approx 10^8 \text{ cm s}^{-1}$  as the typical velocity<sup>5</sup>

In Figure 1 we plot the resulting optical constants for crystalline SNPs, both for neutral SNPs and SNPs with a radius  $a = 10 \text{ \AA}$  and  $Z = +1$ . We see that the hole dominates the absorption for  $\lambda \gtrsim 1 \mu\text{m}$ , and completely overwhelms the weak vibrational bands in the  $7\text{--}25 \mu\text{m}$  region which provide the infrared absorption in neutral Si. For comparison, we also show the optical constants from KKS93.

For glassy  $\text{SiO}_2$ , we take  $m''$  from Palik (1985) for  $0.01 < \lambda < 7 \mu\text{m}$  but with one modification: for  $0.15 < \lambda < 3.6 \mu\text{m}$  we set  $m'' = 1.0 \times 10^{-4}$  based on the absorption coefficient measured by Harrington et al. (1978). For  $7 < \lambda < 500 \mu\text{m}$  we take  $m''$  from Henning & Mutschke (1997) for glassy  $\text{SiO}_2$  sample at 100 K (the optical properties of glassy  $\text{SiO}_2$  are not sensitive to temperature, see Henning & Mutschke 1997). For  $\lambda > 500 \mu\text{m}$ , we approximate  $m''(\lambda) \approx m''(500 \mu\text{m})(500 \mu\text{m}/\lambda)$ . Again, the real part  $m'$  is calculated from the Kramers-Kronig relation. The results are also presented in Figure 1.

In Figure 2 we show the absorption cross sections per unit volume calculated for both spherical and spheroidal (a) pure Si grains, and (b) Si/ $\text{SiO}_2$  grains, with the Si in a confocal spheroidal core containing a fraction  $(0.8)^3 = 51\%$  of the volume. We also plot in Figure 2c the radiation fields for the diffuse ISM and for NGC 2023 ( $60''$  S of HD 37903; see §3.1).

Figures 2a and 2b clearly show that in the wavelength range where Si or Si/ $\text{SiO}_2$  grains absorb most ( $\lambda \lesssim 0.25 \mu\text{m}$ ) the grain shape can substantially affect the wavelength-dependence of the ultraviolet absorption. However, we will see below (§4) that the integrated energy absorption rate, and the resulting emission spectrum, is surprisingly insensitive to grain shape.

## 2.2. Enthalpies

The experimental specific heat of bulk crystalline Si can be approximated by a Debye model (with dimensionality  $n = 3$ ) and Debye temperature  $\Theta = 530 \text{ K}$ , while  $\text{SiO}_2$  glass can be approximated by a model where  $1/3$  of the vibrational modes are distributed according to a Debye model with  $\Theta = 275 \text{ K}$ , and  $2/3$  of the modes according to a Debye model with  $\Theta = 1200 \text{ K}$ .

For very small particles at low temperatures, the discrete nature of the vibrational spectrum becomes important. Let  $N_{\text{atom}}^{\text{Si}}$  and  $N_{\text{atom}}^{\text{SiO}_2}$  be the number of atoms in the Si core and  $\text{SiO}_2$  mantle, and  $N_{\text{atom}} \equiv N_{\text{atom}}^{\text{Si}} + N_{\text{atom}}^{\text{SiO}_2}$  be the total number of atoms. For pure Si clusters, we set  $N_m = 3N_{\text{atom}}^{\text{Si}} - 6$  vibrational modes where the “−6” term allows for the translational and rotational degrees of freedom since the energy from photon absorption is only distributed among the vibrational modes. For Si/ $\text{SiO}_2$  nanoparticles, we assume  $N_m = 3N_{\text{atom}}^{\text{Si}} - 3$  modes distributed according to a  $\Theta = 530 \text{ K}$  Debye model,  $N_m = 2N_{\text{atom}}^{\text{SiO}_2} - 2$  modes distributed according to a  $\Theta = 1200 \text{ K}$  Debye model, and  $N_m = N_{\text{atom}}^{\text{SiO}_2} - 1$  modes distributed according to a  $\Theta = 275 \text{ K}$  Debye model. We assume the mode frequencies to be distributed following eqs.(4-6) and eq.(11) of Draine & Li (2001). The specific heat is calculated treating the modes as harmonic oscillators, with the

---

<sup>4</sup>For a positively charged SNP, the relevant mass is the effective mass of a hole. There are two degenerate valence band maxima, with hole masses  $0.49m_e$  and  $0.16m_e$  (Ashcroft & Mermin 1976, p. 569); we adopt  $0.2m_e$  as a representative value. The conduction band minima are characterized by electron effective masses of 1.0 and  $0.2m_e$ ; these would be relevant for negatively-charged SNPs.

<sup>5</sup>Our estimate of  $\tau$  is by no means exact, but the value of  $\tau$  is unimportant in the case of oxide-coated SNPs, since the oxide layer dominates the IR emission. As mentioned above, interstellar SNPs are thought to be oxide-coated.

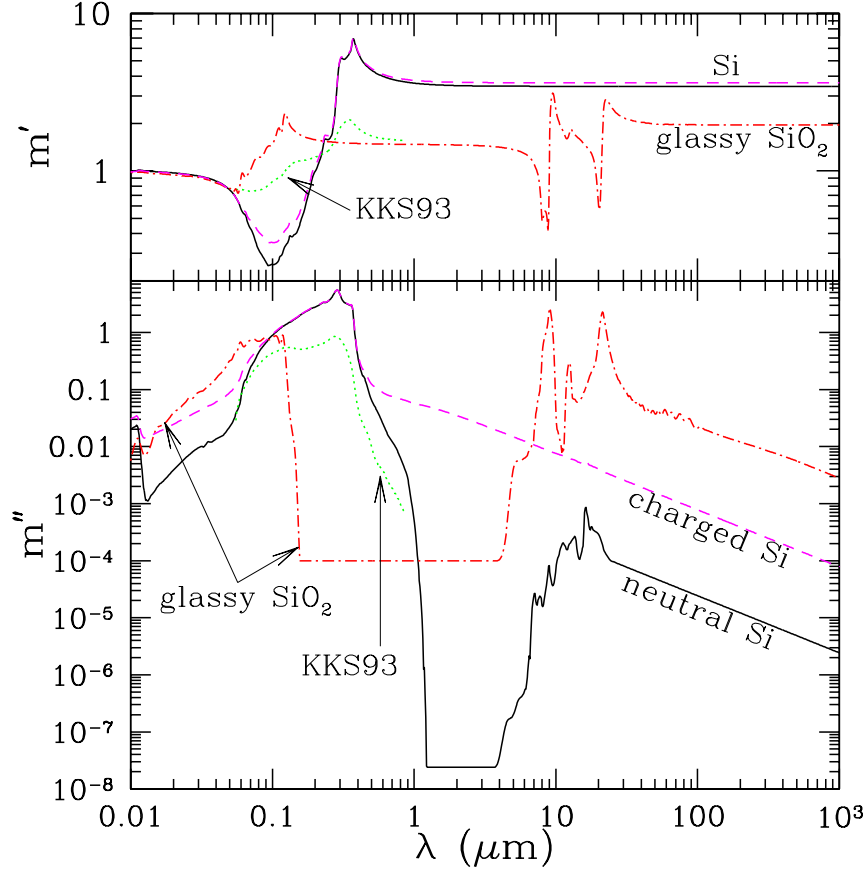


Fig. 1.— Optical constants  $m'$  (upper panel),  $m''$  (lower panel) of neutral Si (solid lines), charged Si ( $Z = +1$ ,  $a = 10 \text{ \AA}$ ; dashed lines), and  $\text{SiO}_2$  glass (dot-dashed lines). Also plotted are those of Koshida et al. 1993 (dotted lines; labelled by KKS93).

continuum limit used for large particles and high energies (see Draine & Li 2001).

### 3. IR Emission Spectrum and Its Implications

Let  $Z_{\text{Si}}$  be the amount of Si in the grains (by number) relative to total hydrogen. The IR emissivity per unit solid angle per H nucleon from the SNPs is

$$j_{\lambda}(a) = \frac{Z_{\text{Si}}}{N_{\text{Si}}(a)} C_{\text{abs}}(a, \lambda) \int_0^{\infty} dT B_{\lambda}(T) P(a, T) \quad (3)$$

where  $N_{\text{Si}}(a)$  is the number of Si atoms in a grain of radius  $a$  [ $N_{\text{Si}} = (\pi a^3 / 21 m_{\text{H}}) \rho_{\text{Si}}$  for pure Si nanoparticles, and  $N_{\text{Si}} = \pi a_{\text{Si}}^3 \rho_{\text{Si}} / 21 m_{\text{H}} + \pi (a^3 - a_{\text{Si}}^3) \rho_{\text{SiO}_2} / 45 m_{\text{H}}$  for grains with Si cores of radius  $a_{\text{Si}}$  and  $\text{SiO}_2$  mantles, where  $\rho_{\text{Si}}$ ,  $\rho_{\text{SiO}_2}$  are the mass densities of crystalline Si ( $\approx 2.42 \text{ g cm}^{-3}$ ) and glassy  $\text{SiO}_2$  ( $\approx 2.2 \text{ g cm}^{-3}$ ), respectively, and  $m_{\text{H}}$  is the mass of a hydrogen atom];  $C_{\text{abs}}(a, \lambda)$  is the absorption cross section of the spheroidal core-mantle grain at wavelength  $\lambda$ , calculated using the optical constants discussed in §2.1;  $B_{\lambda}(T)$  is the Planck function;  $P(a, T) dT$  is the probability that the grain temperature will be in  $[T, T + dT]$ . For a given radiation field, we calculate  $P(a, T)$  for small grains employing the “thermal-discrete” method (Draine

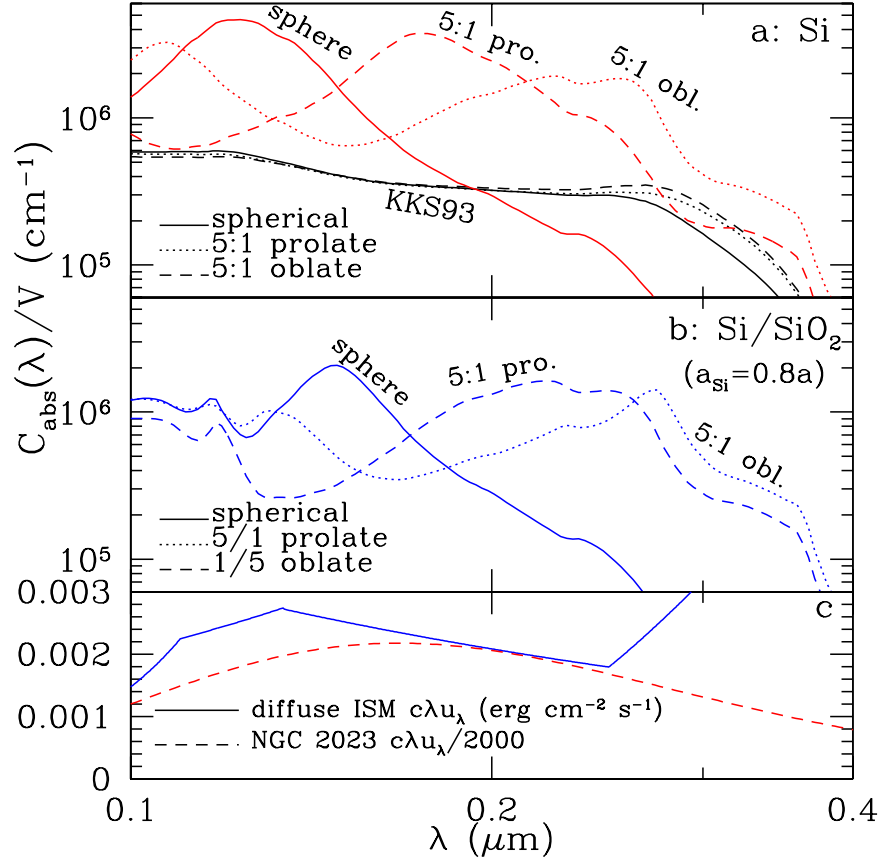


Fig. 2.— (a): Absorption cross sections per unit volume of spherical Si grains (solid line), 5:1 prolate Si grains (dashed line), 5:1 oblate Si grains (dotted line). Also plotted are the spherical, 5:1 prolate, 5:1 oblate grains using the optical constants of Koshida et al. (1993) (labelled by KKS93). (b) Absorption cross sections per unit volume of spherical Si/SiO<sub>2</sub> grains (solid line), 5:1 prolate Si/SiO<sub>2</sub> grains (dashed line), 5:1 oblate Si/SiO<sub>2</sub> grains (dotted line). All grains are taken to have the same Si core volume fraction 51% (for the spherical case,  $a_{\text{Si}} = 0.8a$ ). (c): The solar neighbourhood interstellar radiation field (Mathis, Mezger, & Panagia 1983) and the NGC 2023 radiation field at a position 60'' S of HD 37903 (see §3.1).

& Li 2001).<sup>6</sup> We characterize the intensity of the illuminating starlight by  $\chi$ , the intensity at 1000 Å relative to the Habing (1968) radiation field. For NGC 2023 the spectrum is assumed to be a 22000 K dilute blackbody cutoff at the Lyman edge; for the diffuse interstellar medium we take the spectrum of Mathis, Mezger, & Panagia (1983), with  $\chi = 1.23$ .

### 3.1. NGC 2023

The reflection nebula NGC 2023, at a distance  $D = 450\text{pc}$ , is illuminated by the B1.5V star HD 37903 ( $T_{\text{eff}} = 22,000\text{K}$ ,  $L_{\star} = 7600L_{\odot}$ ). A modest HII region surrounds the star, beyond which is a photodissoci-

<sup>6</sup>To be precise, the energy released in the form of PL is not available as heat. In NGC 2023, with a mean energy  $\langle h\nu \rangle_{\text{ERE}} \approx 1.8\text{eV}$  for ERE photons, the fraction of absorbed photon energy lost to photoluminescence  $\eta_{\text{PL}} \langle h\nu \rangle_{\text{ERE}} / \langle h\nu \rangle_{\text{abs}}$  is only  $0.21\eta_{\text{PL}}$  for pure Si ( $\langle h\nu \rangle_{\text{abs}} = 8.6\text{eV}$ ) or  $0.19\eta_{\text{PL}}$  for SiO<sub>2</sub>-coated Si ( $\langle h\nu \rangle_{\text{abs}} = 9.3\text{eV}$ ). Even for  $\eta_{\text{PL}} \rightarrow 1$ , this is a minor correction which does not alter our conclusions.

ation region at an estimated distance  $\sim 5 \times 10^{17}$  cm from the star. The radiation field is expected to have an intensity  $\chi \approx 5000$  at this distance from the star. While  $\chi \approx 5000$  is consistent with models to reproduce the observed IR and far-red emission from UV-pumped  $\text{H}_2$  in the bright “emission bar”  $80''$  S of HD 37903 (Draine & Bertoldi 1996, 2000), the integrated infrared 5–60  $\mu\text{m}$  surface brightness at a position  $60''$  S of HD 37903 (Figure 5) points to a lower value of  $\chi$ . We will assume that the dust producing the measured infrared spectrum and ERE is illuminated by a radiation field with  $\chi \approx 2000$ .<sup>7</sup>

In Figures 3 and 4 we show temperature distribution functions  $P(a, T)$  for pure Si nanoparticles and Si/SiO<sub>2</sub> nanoparticles of various sizes. In each case we show  $P(a, T)$  for both neutral and charged grains.

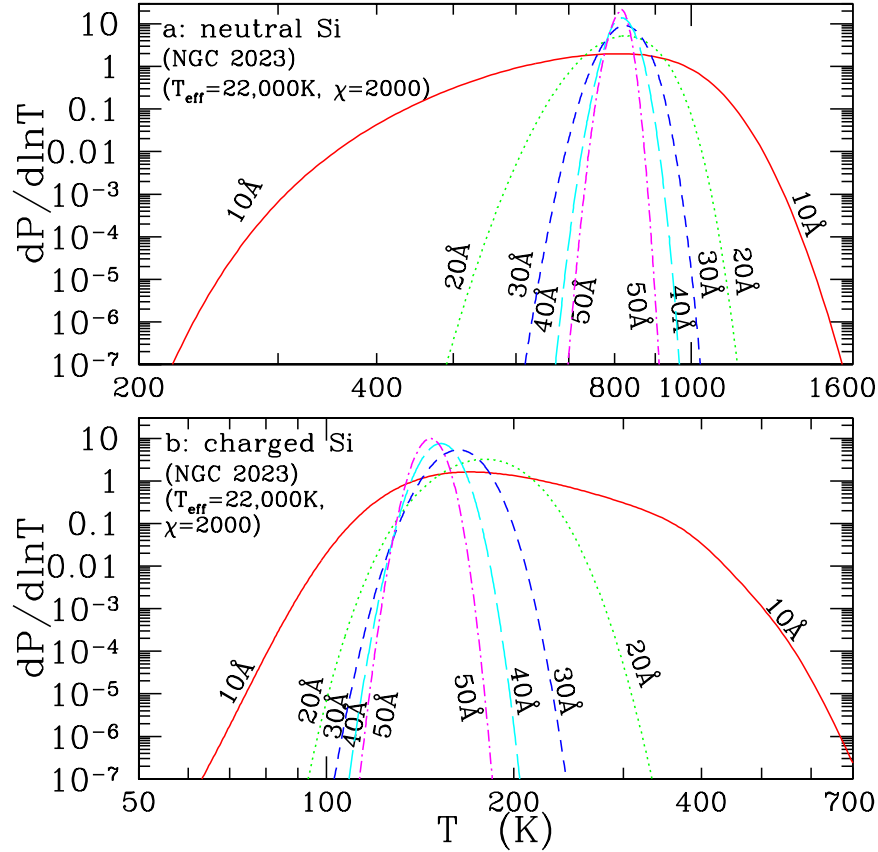


Fig. 3.— Temperature distribution functions for pure Si spheres of various radii, using the optical properties of (a) neutral particles and (b) particles with charge  $Z = +1$ , exposed to the radiation field in NGC 2023. Curves are labelled by grain radius  $a$ .

The 2.4–45  $\mu\text{m}$  spectrum has been obtained by Verstraete et al. (2001) using the Infrared Space Observatory, using apertures ranging from  $14'' \times 20''$  (for 2.4–12  $\mu\text{m}$ ) to  $20'' \times 33''$  (for 29–45  $\mu\text{m}$ ), at a position  $60''$  S of HD 37903. Far-infrared photometry with a  $37''$  beam centered  $60''$  S of HD 37903 has been obtained from the Kuiper Airborne Observatory by Harvey et al. (1980). The observed IR spectrum is shown in Figure 5. Proposed ERE carriers must not produce IR emission in excess of what is observed.

The PDR in NGC 2023 is optically thick to the illuminating starlight. Allowing for forward scattering,

<sup>7</sup>As explained in §4, our analysis is insensitive to the precise value assumed for  $\chi$ .

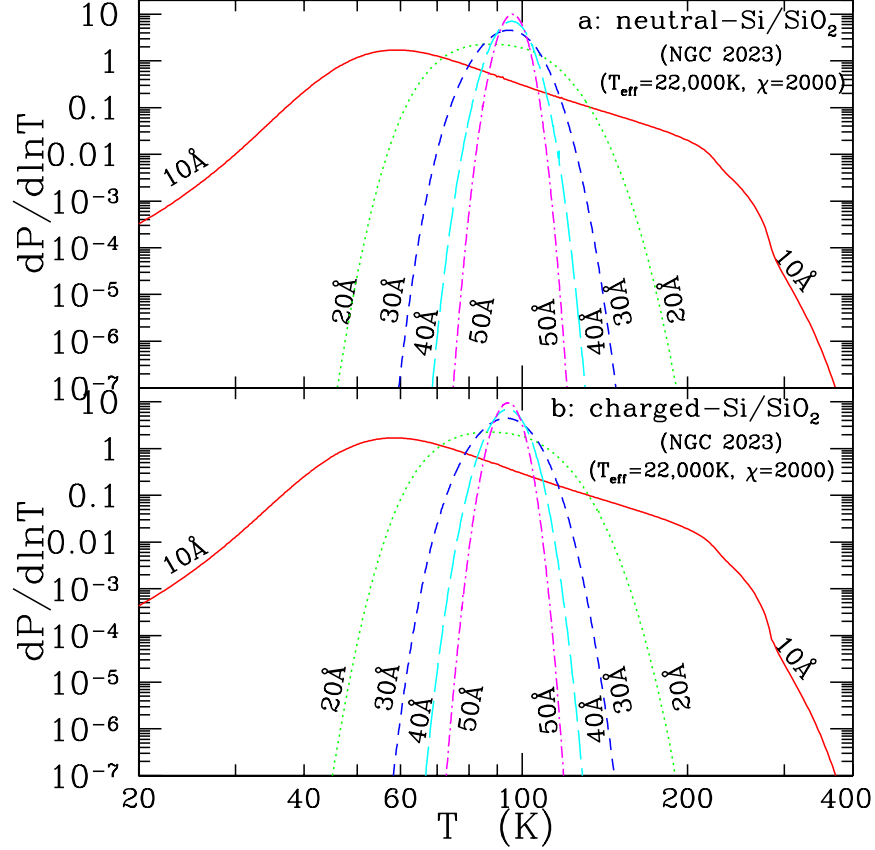


Fig. 4.— Temperature distribution functions for Si/SiO<sub>2</sub> spheres of various radii, with the Si cores assumed to be (a) neutral and (b) charged with  $Z = +1$ , for grains exposed to the radiation field in NGC 2023. Curves are labelled by the Si core radius  $a_{\text{Si}} (\approx 0.8a$  where  $a$  is the Si/SiO<sub>2</sub> radius).

we estimate that the effective attenuation cross section per H nucleon for 3–11 eV photons is  $\sim 0.5 \times 10^{-21} \text{ cm}^2 \text{ H}^{-1}$ , and we approximate the PDR as a slab of optically-thin dust and gas with  $N_{\text{H}} \approx 2 \times 10^{21} \text{ cm}^{-2}$ . We further assume a limb-brightening factor  $1/\cos\theta \approx 2$ , where  $\theta$  is the angle between the slab normal and our line-of-sight (our final results are insensitive to the adopted values of  $N_{\text{H}}$  and  $1/\cos\theta$ ; see §4). With the above assumptions,  $j_{\lambda}$ , the power radiated per H nucleon per unit solid angle per unit wavelength  $\lambda$  (see eq.[3]) is related to the observed intensity  $I_{\lambda}$  by

$$I_{\lambda} = \frac{N_{\text{H}}}{\cos\theta} j_{\lambda} 10^{-0.4A_{\lambda}} \approx 4 \times 10^{21} \text{ cm}^{-2} j_{\lambda} 10^{-0.4A_{\lambda}} \quad (4)$$

where  $A_{\lambda}$  is the extinction between the point of emission and the observer.

The foreground extinction  $A_{\lambda}$  is uncertain. The line-of-sight to HD 37903 has  $E(B - V) \approx 0.35$  and  $R_V \equiv A_V/E(B - V) = 4.1$  (Cardelli, Clayton, & Mathis 1989), corresponding to  $A_{0.68\mu\text{m}} \approx 1.2$ . For the emission bar 80'' S of HD 37903, an extinction  $A_{0.68\mu\text{m}} \approx 3.2$  has been determined from the relative strengths of K band and far-red H<sub>2</sub> emission lines (Draine & Bertoldi 2000). For purposes of discussion, we will assume that the extinction to the reflection region 60'' S of HD 37903 (where the ERE has been measured) is likely to be in the range  $1.2 \lesssim A_{0.68\mu\text{m}} \lesssim 3.2$ .

To estimate  $I^{\text{ERE}}_{\lambda} (\equiv \int I^{\text{ERE}}_{\lambda} d\lambda)$  60'' S of HD37903, we take (1) the measured surface brightness profile



from Witt, Schild, & Kraiman (1984, Figure 7); (2)  $I_{0.68\mu\text{m}}/I_{0.62\mu\text{m}} = 10^{0.06} F_{0.68\mu\text{m}}^*/F_{0.62\mu\text{m}}^* = 0.91$  80'' S of HD37903, where  $F_{\lambda}^*$  is the observed stellar flux (Witt & Schild 1988, Table 1); (3) the ERE spectral profiles 62'' and 84'' ENE of HD37903 (Witt & Boroson 1990, Figure 4).<sup>8</sup> From this we estimate  $I^{\text{ERE}} \approx 9 \times 10^{-5} \text{ erg cm}^{-2} \text{ s}^{-1} \text{ sr}^{-1}$  60'' S of HD37903. The ERE emissivity per H nucleon is

$$j^{\text{ERE}} \equiv \int j_{\lambda}^{\text{ERE}} d\lambda = \frac{\int I_{\lambda}^{\text{ERE}} 10^{0.4A_{\lambda}} d\lambda}{N_{\text{H}}/\cos\theta} \approx 2.3 \times 10^{-26} 10^{0.4A_{0.68\mu\text{m}}} \text{ erg s}^{-1} \text{ sr}^{-1} \text{ H}^{-1} \quad (5)$$

Proposed ERE carriers must provide this level of emission.

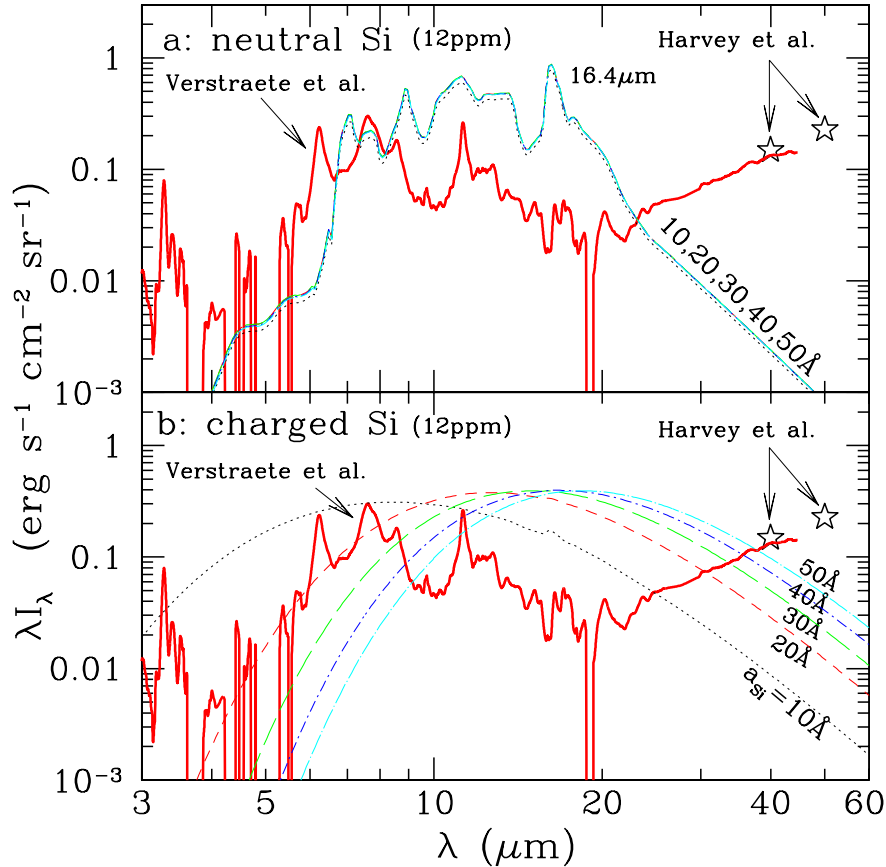


Fig. 5.— Predicted IR emission spectrum for Si/H=12 ppm in (a) neutral and (b)  $Z = +1$  pure Si nanoparticles in NGC 2023. For the neutral Si nanoparticles, the emission is nearly independent of particle size; for the charged Si nanoparticles, spectra are labelled by grain radius. Heavy solid line: ISO SWS spectrum (Verstraete et al. 2001). Stars: KAO photometry (Harvey et al. 1980). For the 16.4 $\mu\text{m}$  feature not to exceed the ISO spectrum, the upper limit on neutral Si SNPs is Si/H  $\lesssim 0.8$  ppm. The upper limit on charged Si SNPs alone is Si/H  $\lesssim 1.5$  ppm. The upper limit on Si SNPs (both neutral and charged) is Si/H  $\lesssim 1.5$  ppm.

<sup>8</sup>The ERE spectrum for 60'' S peaks at 6800 Å (Witt & Schild 1988) as do the spectra 62'' and 84'' ENE of HD37903.

### 3.1.1. Si Nanoparticles

We first calculate the IR emission spectra for crystalline Si grains illuminated by radiation from HD 37903 with intensity  $\chi = 2000$ . As shown in Figure 3, the radiation field is so strong that neutral Si grains with  $a \gtrsim 30\text{\AA}$  attain a steady-state temperature  $\approx 820\text{ K}$ , while  $a \gtrsim 30\text{\AA}$  charged Si grains are heated to  $\lesssim 200\text{ K}$ . The single-photon heating effect (Greenberg 1968) is evident for  $a_{\text{Si}} = 10\text{\AA}$ . In Figure 5 we present the predicted spectra for  $Z_{\text{Si}} = 12\text{ ppm}$  in Si nanoparticles<sup>9</sup> with radii  $a = 10, 20, 30, 40, 50\text{\AA}$ . Grains with  $a \lesssim 100\text{\AA}$  are in the Rayleigh limit for  $\lambda > 912\text{\AA}$ , and thus their “equilibrium” temperatures are independent of  $a$ ; therefore, for a given nanoparticle abundance  $Z_{\text{Si}}$ , the resulting IR intensity is almost independent of grain size.

Although the fundamental lattice vibration of crystalline Si has no dipole moment and thus is IR inactive (i.e., there is no interaction between a single phonon and IR radiation), multi-phonon processes produce prominent bands at  $6.91, 7.03, 7.68, 8.9, 11.2, 13.5, 14.5, 16.4$ , and  $17.9\mu\text{m}$  (Johnson 1959). As seen in Figure 5a, for  $Z_{\text{Si}} = 12\text{ ppm}$  the  $16.4\mu\text{m}$  emission feature is calculated to be about 15 times stronger than the observed spectrum if the grains remain neutral. In order not to exceed the observed spectrum near  $16.4\mu\text{m}$ , NGC 2023 must have  $Z_{\text{Si}} \lesssim 0.8\text{ ppm}$  in neutral Si SNPs – less than  $1/15$  of the abundance of SNPs to explain the ERE in the diffuse ISM. If, however, the pure Si particles have charge  $+1$ , then the thermal emission from the hole results in an emission continuum peaking near  $15\text{--}20\mu\text{m}$ . We see from Figure 5 that an abundance  $Z_{\text{Si}} = 12\text{ ppm}$  in charged SNPs would result in emission which would exceed the observed spectrum by about a factor  $\sim 10$  near  $20\mu\text{m}$ . Thus we obtain an upper limit  $Z_{\text{Si}} \lesssim 1.5\text{ ppm}$  in pure Si SNPs (all charge states) in NGC 2023.

Let  $\eta_{\text{PL}}$  be the photoluminescence efficiency,  $\gamma_{\text{Si}}$  be the UV/visual photon absorption rate per Si (in the  $912\text{--}5500\text{\AA}$  wavelength range), and  $\langle h\nu \rangle_{\text{ERE}}$  be the mean energy of ERE photons. Since the NGC 2023 ERE peaks at  $\sim 6800\text{\AA}$  (Witt & Boroson 1990), we take  $\langle h\nu \rangle_{\text{ERE}} \approx 1.8\text{ eV}$ . Illuminated by starlight of  $T_{\text{eff}}=22,000\text{ K}$ , we calculate  $\gamma_{\text{Si}} \approx 7.43 \times 10^{-6}(\chi/2000)\text{ s}^{-1}\text{ Si}^{-1}$  for neutral Si nanoparticles. The ERE emissivity per H is then  $j^{\text{ERE}} = \langle h\nu \rangle_{\text{ERE}}\gamma_{\text{Si}}\eta_{\text{PL}}Z_{\text{Si}}/4\pi \approx 1.70 \times 10^{-18}\eta_{\text{PL}}Z_{\text{Si}}\text{ erg s}^{-1}\text{ sr}^{-1}\text{ H}^{-1}$ . From eq. (5) we thus require  $\eta_{\text{PL}}Z_{\text{Si}} \approx 1.35 \times 10^{-8}10^{0.4A_{0.68\mu\text{m}}}$ . Correspondingly, for charged Si particles, we obtain  $\gamma_{\text{Si}} \approx 7.04 \times 10^{-6}(\chi/2000)\text{ s}^{-1}\text{ Si}^{-1}$ ,  $j^{\text{ERE}} \approx 1.62 \times 10^{-18}\eta_{\text{PL}}Z_{\text{Si}}\text{ erg s}^{-1}\text{ sr}^{-1}\text{ H}^{-1}$ , and  $\eta_{\text{PL}}Z_{\text{Si}} \approx 1.42 \times 10^{-8}10^{0.4A_{0.68\mu\text{m}}}$ . Results are summarized in Table 1.

Since we have seen that  $Z_{\text{Si}} \lesssim 0.8\text{ ppm}$ , it follows that pure Si neutral nanoparticles could produce the observed ERE only if the photoluminescence efficiency  $\eta_{\text{PL}} \gtrsim 0.017 \times 10^{0.4A_{0.68\mu\text{m}}}$ . For charged Si grains ( $Z_{\text{Si}} \lesssim 1.5\text{ ppm}$ ),  $\eta_{\text{PL}} \gtrsim 0.010 \times 10^{0.4A_{0.68\mu\text{m}}}$  is required. However, according to Smith & Witt (2001), those charged grains will not emit ERE, i.e.,  $\eta_{\text{PL}} \approx 0$ .

### 3.1.2. Si/SiO<sub>2</sub> Nanoparticles

It seems unlikely that *pure* Si nanoparticles would exist in interstellar space without some degree of oxidation. Si nanocrystals in air spontaneously form an overlayer of SiO<sub>2</sub> which is usually  $\sim 10\text{\AA}$  thick (Ledoux et al. 1998). Witt et al. (1998) propose that SNPs in the form of Si core-SiO<sub>2</sub> mantle structure are a product of the initial dust formation process in oxygen-rich stellar mass outflows. Laboratory studies show

---

<sup>9</sup>As discussed in §3.2, we estimate that the observed ERE from the diffuse ISM would require  $Z_{\text{Si}} \geq 12\text{ ppm}$  in Si SNPs, or  $Z_{\text{Si}} \geq 15\text{ ppm}$  in Si/SiO<sub>2</sub> SNPs.

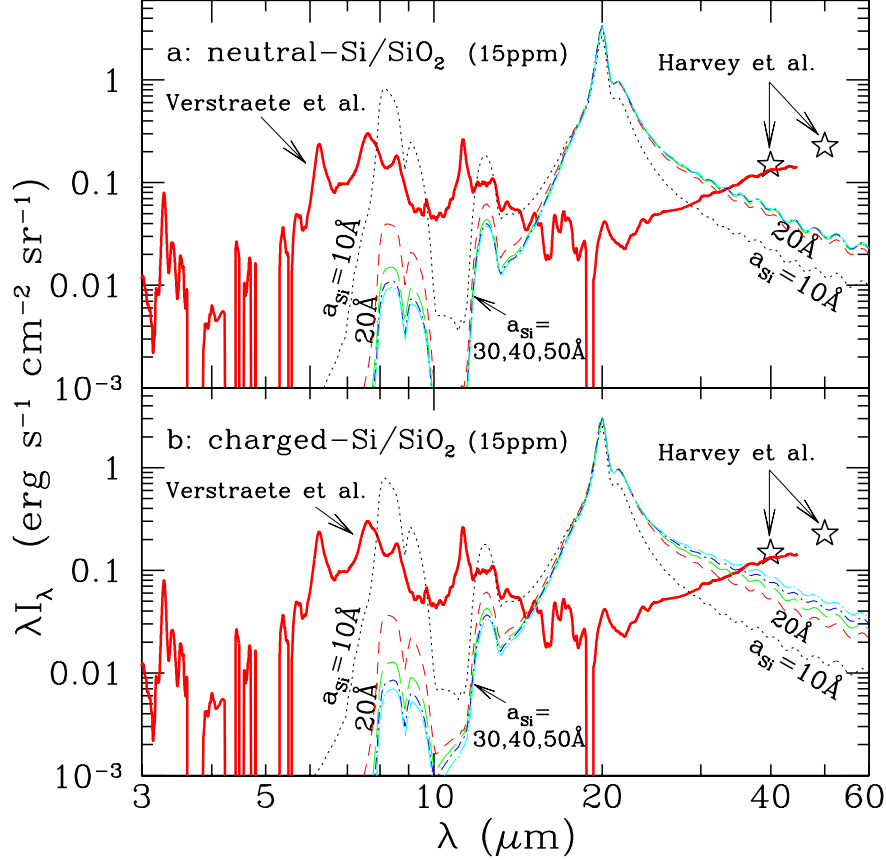


Fig. 6.— As in Figure 5, but for Si/SiO<sub>2</sub> SNPs, for various values of the Si core radius  $a_{\text{Si}} = 0.8a$ . Upper panel (a) – Model spectra calculated for neutral Si/SiO<sub>2</sub> grains containing Si/H=15 ppm, with radii  $a_{\text{Si}} = 10, 20, 30, 40, 50 \text{ \AA}$  (see text). Spectra for  $a_{\text{Si}} = 20, 30, 40, 50 \text{ \AA}$  are nearly indistinguishable. Lower panel (b) – As in (a), but for charged Si/SiO<sub>2</sub> grains. The ripple features at  $\lambda > 30 \mu\text{m}$  are caused by the SiO<sub>2</sub> optical constants adopted from Henning & Mutschke (1998).

that the oxidation of the Si core is a self-limiting process and, in the final stage of oxidation, the thickness of the oxide layer represents about 10% of the total particle diameter (Ledoux et al. 2000).

We now calculate the IR emission spectra for Si core-SiO<sub>2</sub> mantle particles (both neutral and charged). Following Ledoux et al. (2000), we assume  $a_{\text{Si}} = 0.8a$  where  $a_{\text{Si}}$  and  $a$  are respectively the radii of the Si core and the Si/SiO<sub>2</sub> entire grain. In Figure 6 we show theoretical spectra for  $a_{\text{Si}} = 10, 20, 30, 40, 50 \text{ \AA}$  with  $Z_{\text{Si}} = 15 \text{ ppm}$  (estimated in §3.2 for Si/SiO<sub>2</sub> grains to account for the ERE in the diffuse ISM) together with the observed spectrum for NGC 2023. As illustrated in Figure 6 the Si-O modes produce strong features at  $20 \mu\text{m}$ ,  $12.5 \mu\text{m}$  and  $9.1 \mu\text{m}$ . The most conspicuous feature is the strong and broad  $20 \mu\text{m}$  band which, for  $Z_{\text{Si}} = 15 \text{ ppm}$ , is  $\sim 80$  times stronger than the observational data. To depress the  $20 \mu\text{m}$  emission feature to a level not in contradiction with the observational spectrum, NGC 2023 must have  $Z_{\text{Si}} \lesssim 0.2 \text{ ppm}$  in SiO<sub>2</sub>-coated Si grains (all charge states).

The  $912\text{--}5500 \text{ \AA}$  photon absorption rate for these Si/SiO<sub>2</sub> neutral SNPs is  $\gamma_{\text{Si}} \approx 6.19 \times 10^{-6} (\chi/2000) \text{ s}^{-1} \text{ Si}^{-1}$ . The ERE emissivity per H is then  $\langle h\nu \rangle_{\text{ERE}} \gamma_{\text{Si}} \eta_{\text{PL}} Z_{\text{Si}} / 4\pi \approx 1.42 \times 10^{-18} \eta_{\text{PL}} Z_{\text{Si}} \text{ erg s}^{-1} \text{ sr}^{-1} \text{ H}^{-1}$ . From eq. (5) we thus require  $\eta_{\text{PL}} Z_{\text{Si}} \approx 1.62 \times 10^{-8} 10^{0.4A_{0.68\mu\text{m}}}$ . Since  $Z_{\text{Si}} \lesssim 0.2 \text{ ppm}$  the *observed* ERE intensity in NGC 2023 (eq.[5]) requires a photoluminescence efficiency  $\eta_{\text{PL}} \gtrsim 0.081 \times 10^{0.4A_{0.68\mu\text{m}}}$  if due to

Si core-SiO<sub>2</sub> mantle neutral nanoparticles. Similarly, we obtain for Si/SiO<sub>2</sub> charged SNPs  $\gamma_{\text{Si}} \approx 6.00 \times 10^{-6}(\chi/2000) \text{ s}^{-1} \text{ Si}^{-1}$ ,  $j^{\text{ERE}} \approx 1.37 \times 10^{-18} \eta_{\text{PL}} Z_{\text{Si}} \text{ erg s}^{-1} \text{ sr}^{-1} \text{ H}^{-1}$ ,  $\eta_{\text{PL}} Z_{\text{Si}} \approx 1.68 \times 10^{-8} 10^{0.4A_{0.68\mu\text{m}}}$ , and  $\eta_{\text{PL}} \gtrsim 0.084 \times 10^{0.4A_{0.68\mu\text{m}}}$ . Again, according to Smith & Witt (2001), those charged grains will have  $\eta_{\text{PL}} \approx 0$ . Results are also summarized in Table 1.

### 3.2. Diffuse Interstellar Medium

Using Pioneer 10 and 11 observations, Gordon et al. (1998) estimated the ERE emissivity per H nucleon of the high Galactic latitude (HGL) diffuse ISM to be  $j^{\text{ERE}} \approx 1.4 \times 10^{-26} \text{ erg s}^{-1} \text{ sr}^{-1} \text{ H}^{-1}$ . Szomoru & Guhathakurta (1998) obtained  $\langle I^{\text{ERE}} \rangle = 1.2 \times 10^{-5} \text{ erg s}^{-1} \text{ sr}^{-1} \text{ cm}^{-2}$  toward 3 cirrus clouds with  $\langle N_{\text{H}} \rangle = 7.3 \times 10^{20} \text{ cm}^{-2}$ , giving  $j^{\text{ERE}} \approx 1.6 \times 10^{-26} \text{ erg s}^{-1} \text{ sr}^{-1} \text{ H}^{-1}$ . Evidently the ERE carrier must provide an emissivity  $j^{\text{ERE}} \approx 1.5 \times 10^{-26} \text{ erg s}^{-1} \text{ sr}^{-1} \text{ H}^{-1}$  in the diffuse ISM. The ERE appears to peak at  $\sim 6000 \text{ \AA}$  (Szomoru & Guhathakurta 1998); if due to SNPs, this would indicate  $2a \approx 28 \text{ \AA}$  (Ledoux et al. 2000), or  $a_{\text{Si}} \approx 0.8a \approx 11 \text{ \AA}$ .

#### 3.2.1. Si Nanoparticles

The 912–5500Å photon absorption rates  $\gamma_{\text{Si}}$  for pure Si neutral and charged grains are  $\approx 4.94 \times 10^{-9}(\chi/1.23) \text{ s}^{-1} \text{ Si}^{-1}$ , and  $\approx 4.68 \times 10^{-9}(\chi/1.23) \text{ s}^{-1} \text{ Si}^{-1}$ , respectively. Thus  $j^{\text{ERE}} \approx 1.32 \times 10^{-21}(\chi/1.23) \eta_{\text{PL}} Z_{\text{Si}} \text{ erg s}^{-1} \text{ sr}^{-1}$  and  $j^{\text{ERE}} \approx 1.25 \times 10^{-21}(\chi/1.23) \eta_{\text{PL}} Z_{\text{Si}} \text{ erg s}^{-1} \text{ sr}^{-1} \text{ H}^{-1}$ , respectively, for neutral and charged Si grains. Therefore, since  $\eta_{\text{PL}} \leq 100\%$ , we require  $Z_{\text{Si}} \gtrsim 12 \text{ ppm}$  ( $\gtrsim 33\%$  of  $[\text{Si}/\text{H}]_{\odot}$ ) for both neutral and charged Si grains. In Figure 7 we plot the temperature probability distribution functions for these grains, and IR emission spectra are shown in Figure 8.

The DIRBE 25μm photometry is inconsistent with  $Z_{\text{Si}} \approx 12 \text{ ppm}$  in pure Si neutral nanoparticles, with an upper limit  $Z_{\text{Si}} \lesssim 4 \text{ ppm}$ . For charged Si grains, the predicted IR spectra are not in conflict with the DIRBE photometry. However, we note again that, according to Smith & Witt (2001), those charged grains will not emit ERE. Results are summarized in Table 1.

#### 3.2.2. Si/SiO<sub>2</sub> Nanoparticles

Similarly, we have also considered Si core-SiO<sub>2</sub> mantle grains with  $a_{\text{Si}} = 0.8a$ , assuming the Si core to be either neutral or have charge +1.

The 912–5500Å photon absorption rates  $\gamma_{\text{Si}}$  for Si/SiO<sub>2</sub> neutral and charged grains are  $\approx 3.87 \times 10^{-9}(\chi/1.23) \text{ s}^{-1} \text{ Si}^{-1}$ , and  $\approx 3.77 \times 10^{-9}(\chi/1.23) \text{ s}^{-1} \text{ Si}^{-1}$ , respectively. Thus  $j^{\text{ERE}} \approx 1.04 \times 10^{-21}(\chi/1.23) \eta_{\text{PL}} Z_{\text{Si}} \text{ erg s}^{-1} \text{ sr}^{-1}$  and  $j^{\text{ERE}} \approx 1.00 \times 10^{-21}(\chi/1.23) \eta_{\text{PL}} Z_{\text{Si}} \text{ erg s}^{-1} \text{ sr}^{-1} \text{ H}^{-1}$ , respectively, for neutral and charged Si/SiO<sub>2</sub> grains. Therefore, since  $\eta_{\text{PL}} \leq 100\%$ , we require  $Z_{\text{Si}} \gtrsim 15 \text{ ppm}$  ( $\gtrsim 42\%$  of  $[\text{Si}/\text{H}]_{\odot}$ ) for Si/SiO<sub>2</sub> grains. In Figure 9 we plot the temperature probability distribution functions for these grains, and IR emission spectra are shown in Figure 10. Results are also summarized in Table 1.

Evidently, the DIRBE photometry rules out  $Z_{\text{Si}} \approx 15 \text{ ppm}$  in Si/SiO<sub>2</sub> nanoparticles (both neutral and charged) with radii  $a_{\text{Si}} \lesssim 35 \text{ \AA}$ . The DIRBE photometry places an upper limit  $Z_{\text{Si}} \lesssim 2 \text{ ppm}$  on the abundance of the  $a_{\text{Si}} \approx 11 \text{ \AA}$  particle size which appears to be required by the observed wavelength of peak emission in

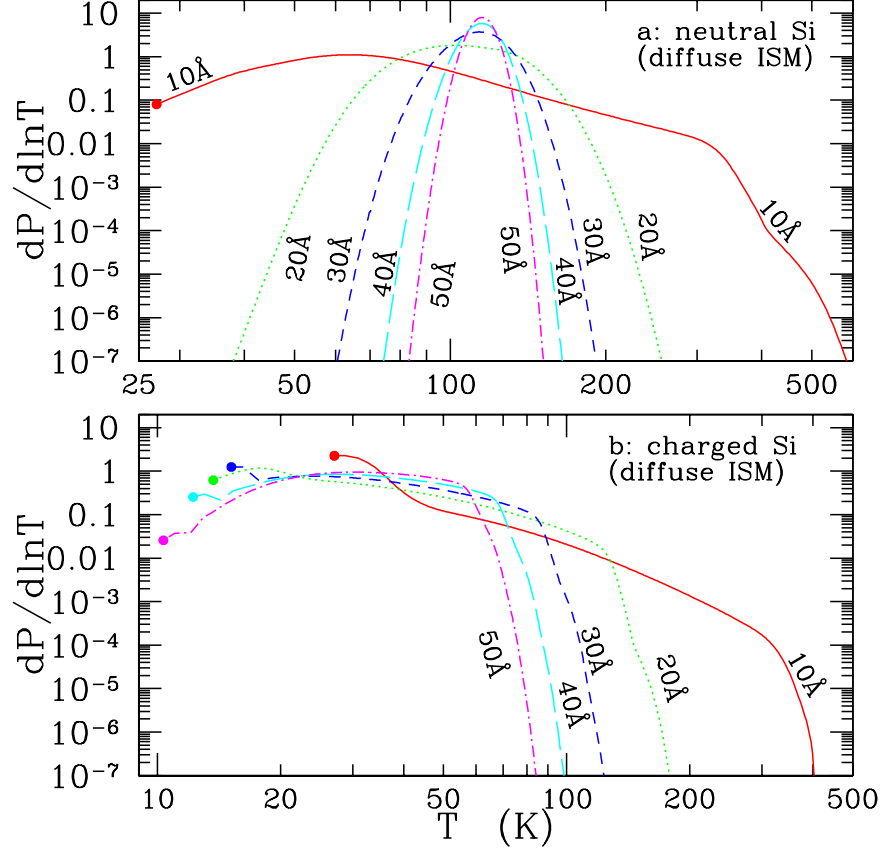


Fig. 7.— Temperature distribution functions for pure Si grains illuminated by the local interstellar radiation field (Mathis, Mezger, & Panagia 1983). Upper panel: neutral Si grains. Lower panel: charged Si grains. For 10 Å (upper panel), 10–50 Å (lower panel) a dot indicates the first vibrationally-excited state (see Draine & Li 2001).

the diffuse ISM. Thus, we conclude that free-flying SNPs can account for no more than 13% of the observed ERE from the diffuse ISM.

SIRTF will be able to obtain diffuse interstellar cloud emission spectra which should either detect the 16.4 or 20  $\mu$ m spectral features, or place much stronger constraints on the abundance of SNPs.

#### 4. Discussion

Si/SiO<sub>2</sub> core-mantle grains are heated primarily by absorption by the Si core (the photoluminescence of which is responsible for the ERE), since the SiO<sub>2</sub> mantle is almost nonabsorptive for  $0.12 \lesssim \lambda \lesssim 4 \mu\text{m}$ ; the core-mantle grains are cooled primarily by the SiO<sub>2</sub> mantle, since  $m''$  is so small for Si in the infrared (see Figure 1). Therefore, increasing the amount of SiO<sub>2</sub> present (while holding the pure Si cores constant) will lead to only small changes in the IR emission resulting from the small decrease in average grain temperature (e.g., Si/SiO<sub>2</sub> grains with equal numbers of Si atoms in the core and in the mantle [ $a_{\text{Si}} \approx 0.668a$ ] in NGC 2023 [ $\chi=2000$ ] have a steady-state temperature  $\approx 85\text{K}$  in comparison with  $\approx 96\text{K}$  for grains with  $a_{\text{Si}} = 0.8a$ ). The limits on  $\eta_{\text{PL}}$  will be only slightly affected by increasing the thickness of the SiO<sub>2</sub> mantles.

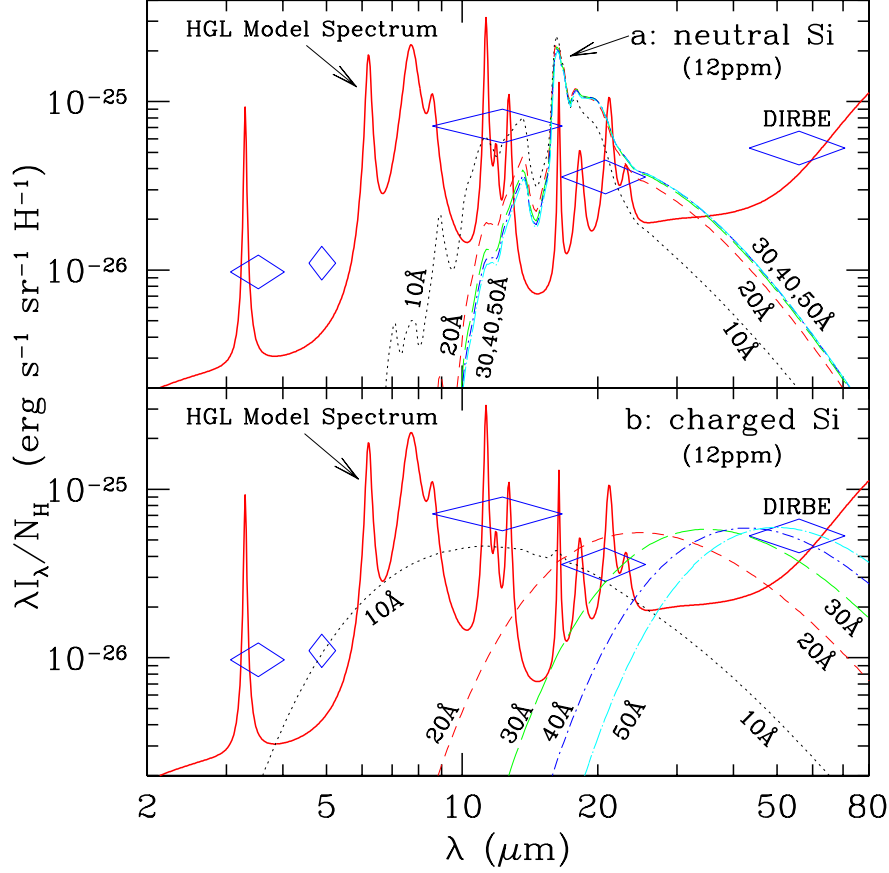


Fig. 8.— Predicted IR emission spectra for pure Si SNPs with  $Z_{\text{Si}} = 12$  ppm in the diffuse ISM, for (a) neutral Si grains, and (b)  $Z = +1$  Si grains. Curves are labelled by grain radius. Also plotted are the DIRBE photometry (diamonds; Arendt et al. 1998) and the HGL model spectrum of Li & Draine (2001).

In §3 the grains are modelled as spherical. To investigate the sensitivity to shape variations, we have also calculated the IR emission spectra for (1) 5:1 prolate grains; (2) 5:1 oblate grains; (3) grains with a distribution of spheroidal shapes with  $dP/dL_{\parallel} = 12L_{\parallel}[1 - L_{\parallel}]^2$  (Ossenkopf, Henning, & Mathis 1992) where  $L_{\parallel}$  is the so-called “depolarization factor” parallel to the grain symmetry axis (for spheres  $L_{\parallel} = 1/3$ ); this shape distribution peaks at spheres and drops to zero for the extreme cases  $L_{\parallel} \rightarrow 0$  (infinitely thin needles) or  $L_{\parallel} \rightarrow 1$  (infinitely flattened pancake). For core-mantle grains, we assume confocal geometry, with the above  $dP/dL_{\parallel}$  applying to the outer surface. For illustration, we present in Figure 11 the IR spectra calculated for neutral Si/SiO<sub>2</sub> grains illuminated by the NGC 2023 radiation field. It is clear that the shape effects are minor: the major change is a slight shift of the peak wavelength of the 20  $\mu\text{m}$  Si-O feature.

In a reflection nebula such as NGC 2023, the IR surface brightness due to SNPs  $\int I_{\lambda} d\lambda \propto N_{\text{H}} \chi Z_{\text{Si}} / \cos \theta$ . While the fraction of the IR power radiated in the 20  $\mu\text{m}$  SiO<sub>2</sub> feature (or the 16.4  $\mu\text{m}$  Si feature in the case of pure Si nanoparticles) depends on  $\chi$  (through the grain temperature), this dependence is relatively weak for modest changes in  $\chi$ . Therefore the upper limits on the 16.4 and 20  $\mu\text{m}$  features in NGC 2023 give upper limits on  $N_{\text{H}} \chi Z_{\text{Si}} / \cos \theta$ ; these limits, plus the observed  $\text{ERE} \propto \eta_{\text{PL}} N_{\text{H}} \chi Z_{\text{Si}} / \cos \theta$  then give lower limits on  $\eta_{\text{PL}}$ , independent of the actual values of  $N_{\text{H}}$  and  $\cos \theta$ , and only weakly dependent on the value of  $\chi$ .

One considerable uncertainty in our analysis concerns the UV absorption properties of nano-Si material.

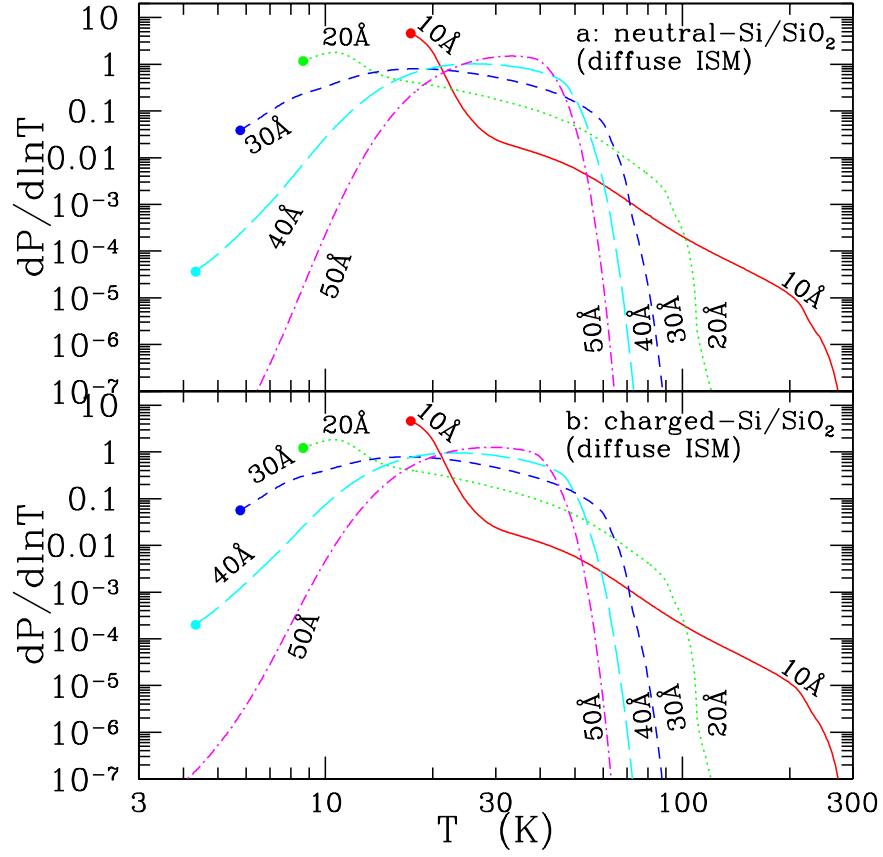


Fig. 9.— Temperature distribution functions for Si/SiO<sub>2</sub> spheres of various radii, with the Si cores assumed to be (a) neutral and (b) charged with  $Z = +1$ , for grains illuminated by the local interstellar radiation field (Mathis, Mezger, & Panagia 1983). Curves are labelled by the Si core radius  $a_{\text{Si}}$  ( $\approx 0.8a$  where  $a$  is the Si/SiO<sub>2</sub> radius). For  $a_{\text{Si}} = 10, 20, 30, 40 \text{ \AA}$  a dot indicates the first excited state (see Draine & Li 2001).

In the literature, it is often stated that, as a result of quantum confinement, the optical-UV absorption of nano-Si is substantially reduced in comparison with those of bulk-Si. If this is true, the SNP model would require an even larger Si abundance to account for the ERE, and the limitations placed on this model would be even more severe.

Another uncertainty concerns the IR emission properties of nano-Si crystals and nano-SiO<sub>2</sub>, which have not yet been experimentally investigated. In the present work, our results are mainly based on the IR emissivities of bulk Si and bulk SiO<sub>2</sub>. Nano-materials are expected to be more IR-active than their bulk counterparts (due to the symmetry-breaking surfaces) and therefore the detailed emission spectrum will be modified. However, the starlight energy absorbed by the grains has to be reradiated in the infrared, so the absence of detected spectral features implies upper limits on the SNP abundance.

Our analysis of NGC 2023 required the value of the foreground extinction  $A_\lambda$  to “deredden” the ERE measurements. Unfortunately,  $A_\lambda$  has not been directly measured at the location where the ERE observations have been made. It would be extremely valuable to have ERE measurements made at a position where a reliable extinction has been determined – such as the emission bar 80'' S of HD 39037 – or to have both IR and far-red observations of H<sub>2</sub> emission (allowing  $A_\lambda$  to be determined) at a location where the ERE has

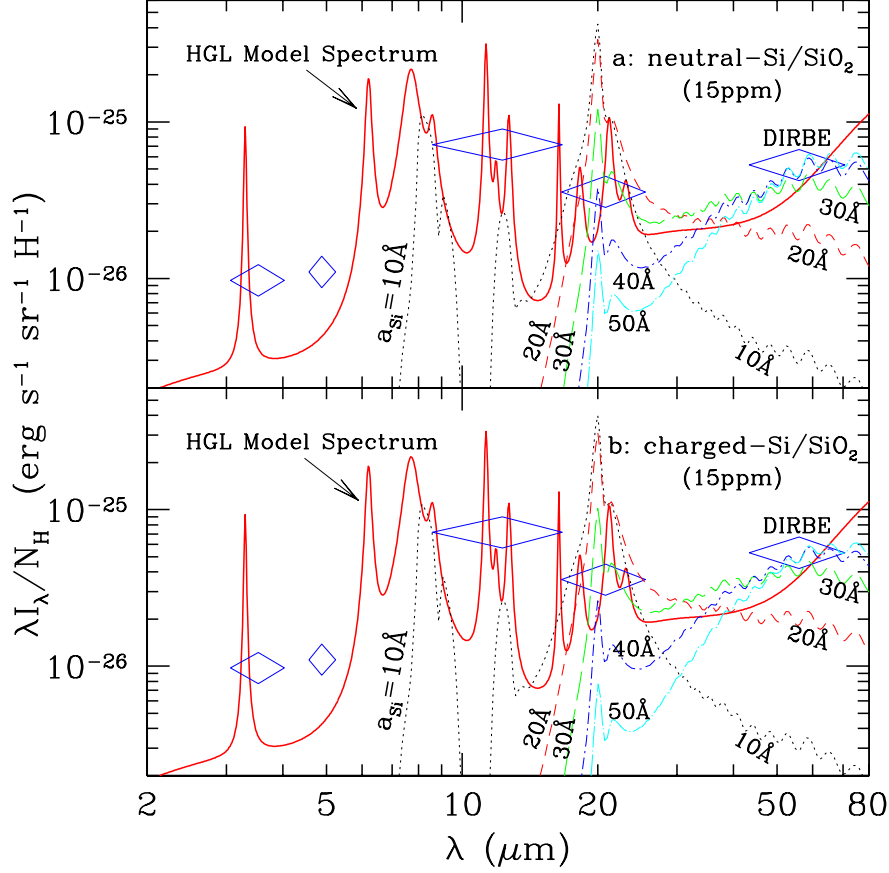


Fig. 10.— As in Fig. 8, but for Si/SiO<sub>2</sub> SNPs with  $Z_{\text{Si}} = 15$  ppm.

been measured.

Our modelling has assumed isolated “free-flying” SNPs; we have demonstrated that existing DIRBE photometry for the diffuse ISM rules out the hypothesis that the observed ERE is due to such particles. Since isolated SNPs are ruled out, it is important to note that in the laboratory, photoluminescence is observed for SNPs located on a substrate (Ledoux et al. 2000). An SNP located on the surface of a large interstellar grain would have its temperature – and therefore its infrared emission – determined by the temperature of the “host” grain. In the case of NGC 2023, the radiation field is so intense that the “host” temperature would probably be similar to the temperature of the Si/SiO<sub>2</sub> SNPs, so the 20  $\mu\text{m}$  SiO<sub>2</sub> emission feature should still be prominent, though its strength could be increased or decreased, depending on the optical properties of the “host” grain. If the SNPs are pure Si, however, the 16.4  $\mu\text{m}$  emissivity would be reduced if the SNPs are attached to a host, since the host grain would not be as hot as the Si SNPs, which are poor thermal emitters. In the diffuse ISM, the 16.4 and 20  $\mu\text{m}$  emission would be completely suppressed if the SNPs are attached to larger host grains, with temperatures  $T \approx 15 - 20$  K. Thus SNPs attached to larger host grains may be a viable explanation for the observed ERE.

The photoexcitation rate  $\gamma$  for SNPs on the surfaces of  $a \gtrsim 100$  Å grains would probably be lower than for free-flying SNPs, which would in turn increase the abundance of Si in SNPs required to explain the observed ERE. Since 42% or more of  $[\text{Si}/\text{H}]_{\odot}$  is required even for free-flying SNPs, the Si abundance



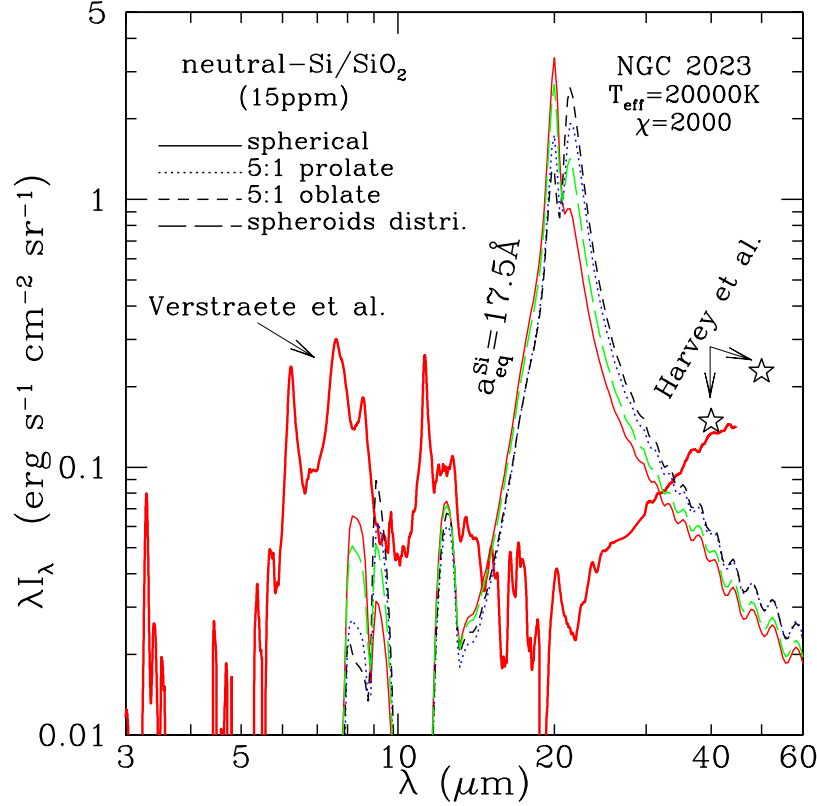


Fig. 11.— Grain shape effects on the model IR emission spectra calculated from spherical grains (thin solid line), 5:1 prolate grains (dotted line), 5:1 oblate grains (short-dashed line), and grains with a distribution of spheroidal shapes (long-dashed line) illuminated by the NGC 2023 radiation field. All grains are taken to (1) be neutral; (2) have an equivalent sphere-volume Si core size  $a_{\text{eq}}^{\text{Si}} = 17.5 \text{ \AA}$  (we choose  $17.5 \text{ \AA}$  because Smith & Witt [2001] found that the observed ERE in the diffuse ISM can be best explained by SNPs with  $a_{\text{Si}} = 17.5 \text{ \AA}$ ); (3) have the Si core taking over 51% of the total grain volume. Also plotted are the ISO SWS spectrum (heavy solid line; Verstraete et al. 2001) and the KAO photometry (stars; Harvey et al. 1980). It is evident that the grain shape effect does not affect our conclusions.

demands would be difficult to accommodate if the SNPs are attached to  $a \gtrsim 100 \text{ \AA}$  grains.

## 5. Conclusions

Table 2 summarizes our results for the abundances of SNPs: upper limits based on nondetection of  $16.4 \mu\text{m}$  and  $20 \mu\text{m}$  features, and lower limits (since  $\eta_{\text{PL}} \leq 1$ ) if neutral SNPs are to account for the observed ERE. Note charged SNPs are not able to emit ERE (Smith & Witt 2001).

For pure (both neutral and charged) Si SNPs, nondetection of a  $16.4 \mu\text{m}$  emission feature in NGC 2023 implies  $\eta_{\text{PL}} \gtrsim 0.017 \times 10^{0.4A_{0.68\mu\text{m}}}$ . Thus for  $A_{0.68\mu\text{m}} = 1.2$ , pure neutral Si SNPs could account for the observed ERE in NGC 2023 provided  $\eta_{\text{PL}} \gtrsim 5\%$ , but if  $A_{0.68\mu\text{m}} = 3.2$ ,  $\eta_{\text{PL}} \gtrsim 32\%$  would be required to account for the ERE. We note in the laboratory high photoluminescence efficiencies are seen only when the Si surfaces are “passivated” by an oxide coating.

An oxide coating, however, will introduce a strong emission feature at  $20 \mu\text{m}$  which is not seen in

Table 1: ERE Emissivities of SNPs

	Item	NGC 2023	Diffuse ISM
Observational	$\langle h\nu \rangle_{\text{ERE}}$ (eV)	1.8	2.1
	$j_{\text{obs}}^{\text{ERE}}$ (erg s <sup>-1</sup> sr <sup>-1</sup> H <sup>-1</sup> ) <sup>a</sup>	$2.3 \times 10^{-26} 10^{0.4A_{0.68\mu\text{m}}}$	$1.5 \times 10^{-26}$
neutral Si	$\langle h\nu \rangle_{\text{abs}}$ (eV) <sup>b</sup>	9.24	9.25
	$\gamma_{\text{Si}}$ (s <sup>-1</sup> Si <sup>-1</sup> ) <sup>c</sup>	$7.43 \times 10^{-6} (\chi/2000)$	$4.94 \times 10^{-9} (\chi/1.23)$
	$j_{\text{mod}}^{\text{ERE}}$ (erg s <sup>-1</sup> sr <sup>-1</sup> H <sup>-1</sup> ) <sup>d</sup>	$1.70 \times 10^{-18} \eta_{\text{PL}} Z_{\text{Si}}$	$1.32 \times 10^{-21} \eta_{\text{PL}} Z_{\text{Si}}$
	$\langle h\nu \rangle_{\text{abs}}$ (eV)	9.30	9.29
charged Si	$\gamma_{\text{Si}}$ (s <sup>-1</sup> Si <sup>-1</sup> )	$7.04 \times 10^{-6} (\chi/2000)$	$4.68 \times 10^{-9} (\chi/1.23)$
	$j_{\text{mod}}^{\text{ERE}}$ (erg s <sup>-1</sup> sr <sup>-1</sup> H <sup>-1</sup> )	$1.62 \times 10^{-18} \eta_{\text{PL}} Z_{\text{Si}}$	$1.25 \times 10^{-21} \eta_{\text{PL}} Z_{\text{Si}}$
	$\langle h\nu \rangle_{\text{abs}}$ (eV)	8.59	8.59
neutral Si/SiO <sub>2</sub>	$\gamma_{\text{Si}}$ (s <sup>-1</sup> Si <sup>-1</sup> )	$6.19 \times 10^{-6} (\chi/2000)$	$3.87 \times 10^{-9} (\chi/1.23)$
	$j_{\text{mod}}^{\text{ERE}}$ (erg s <sup>-1</sup> sr <sup>-1</sup> H <sup>-1</sup> )	$1.42 \times 10^{-18} \eta_{\text{PL}} Z_{\text{Si}}$	$1.04 \times 10^{-21} \eta_{\text{PL}} Z_{\text{Si}}$
	$\langle h\nu \rangle_{\text{abs}}$ (eV)	8.65	8.62
charged-Si/SiO <sub>2</sub>	$\gamma_{\text{Si}}$ (s <sup>-1</sup> Si <sup>-1</sup> )	$6.00 \times 10^{-6} (\chi/2000)$	$3.77 \times 10^{-9} (\chi/1.23)$
	$j_{\text{mod}}^{\text{ERE}}$ (erg s <sup>-1</sup> sr <sup>-1</sup> H <sup>-1</sup> )	$1.37 \times 10^{-18} \eta_{\text{PL}} Z_{\text{Si}}$	$1.00 \times 10^{-21} \eta_{\text{PL}} Z_{\text{Si}}$

<sup>a</sup>For NGC 2023,  $j_{\text{obs}}^{\text{ERE}}$  is estimated assuming a UV-illuminated slab with  $N_{\text{H}} = 2 \times 10^{21} \text{ cm}^{-2}$  with limb-brightening  $1/\cos \theta = 2$  (see text).

<sup>b</sup> $\langle h\nu \rangle_{\text{abs}} \equiv \int_{912\text{\AA}}^{5500\text{\AA}} C_{\text{abs}}(h\nu) cu_{\nu} d\nu / \int_{912\text{\AA}}^{5500\text{\AA}} C_{\text{abs}}(h\nu) (cu_{\nu}/h\nu) d\nu$  where  $cu_{\nu}$  is the starlight intensity.

<sup>c</sup> $\gamma_{\text{Si}} \equiv N_{\text{Si}}^{-1} \int_{912\text{\AA}}^{5500\text{\AA}} C_{\text{abs}}(h\nu) (cu_{\nu}/h\nu) d\nu$ .

<sup>d</sup> $j_{\text{mod}}^{\text{ERE}} = \langle h\nu \rangle_{\text{ERE}} \gamma_{\text{Si}} \eta_{\text{PL}} Z_{\text{Si}} / 4\pi$ .

Table 2: IR Limits on Si/H (ppm) in Silicon Nanoparticles

Region	Composition	neutral Si		charged Si <sup>a</sup>	
		Si/H (ppm) from observed IR emission	Si/H (ppm) from observed ERE intensity <sup>b</sup>	Si/H (ppm) from observed IR emission	Si/H (ppm) from observed ERE intensity <sup>b</sup>
NGC 2023	Pure Si	< 0.8	$0.014 \eta_{\text{PL}}^{-1} \times 10^{0.4A_{0.68\mu\text{m}}}$	< 1.5	$0.014 \eta_{\text{PL}}^{-1} \times 10^{0.4A_{0.68\mu\text{m}}}$
	Si/SiO <sub>2</sub>	< 0.2	$0.016 \eta_{\text{PL}}^{-1} \times 10^{0.4A_{0.68\mu\text{m}}}$	< 0.2	$0.017 \eta_{\text{PL}}^{-1} \times 10^{0.4A_{0.68\mu\text{m}}}$
Diffuse ISM	Pure Si	< 4	$12 \eta_{\text{PL}}^{-1}$	< 12	$12 \eta_{\text{PL}}^{-1}$
	Si/SiO <sub>2</sub>	< 2	$15 \eta_{\text{PL}}^{-1}$	< 2	$15 \eta_{\text{PL}}^{-1}$

<sup>a</sup>Note charged SNPs do not luminesce (i.e.  $\eta_{\text{PL}} = 0$ ).

<sup>b</sup> $\eta_{\text{PL}} < 1$  is the photoluminescence efficiency. Lower limits are obtained by setting  $\eta_{\text{PL}} = 1$ .  $A_{0.68\mu\text{m}}$  is the 60''S NGC 2023 foreground extinction at 0.68 $\mu\text{m}$  (see text).

NGC 2023. For Si/SiO<sub>2</sub> nanoparticles to explain the ERE, nondetection of the 20 $\mu$ m feature requires a luminescence efficiency  $\eta_{\text{PL}} \gtrsim 0.081 \times 10^{0.4A_{0.68\mu\text{m}}}$ . Photoluminescence efficiencies as high as 50% have been reported for Si/SiO<sub>2</sub> nanoparticles (Wilson, Szakowski, & Brus 1993), and in principle  $\eta_{\text{PL}}$  could approach 100%. However, if  $A_{0.68\mu\text{m}} \gtrsim 2.8$ , the ERE could not be due to Si/SiO<sub>2</sub> nanoparticles since the required  $\eta_{\text{PL}}$  would then exceed 100%.

The ERE emissivity of the diffuse ISM (Gordon et al. 1998; Szomoru & Guhathakurta 1998) requires  $\gtrsim 42\%$  [Si/H]<sub>⊙</sub> in neutral Si/SiO<sub>2</sub> SNPs, even for photoluminescence efficiency  $\eta_{\text{PL}} \rightarrow 100\%$ . Such a high abundance of SNPs in the diffuse ISM is difficult to reconcile with the evidence that a substantial fraction of interstellar Si is in fact locked up in amorphous silicate grains (e.g., see Weingartner & Draine 2001). This difficulty is exacerbated if interstellar abundances are significantly subsolar, as has been argued (see Snow & Witt 1996).

We have calculated the IR emission which such particles would produce if they are free-flying. Existing DIRBE 25 $\mu$ m photometry appears to already rule out such high abundances of SNPs, indicating that if SNPs are responsible for the ERE from the diffuse ISM, they must either be in  $a \gtrsim 50$  Å clusters, or attached to larger “host” grains. Future observations by SIRTf will be even more sensitive to the abundance of free-flying SNPs in the diffuse interstellar medium.

In light of the controversy over the optical properties of nano-Si material, we call for further experimental studies to determine the dielectric functions of nano-Si material either directly from nano-Si crystals, or from porous-Si with the effects of voids and surface oxidation well determined and removed.

Finally, we also note that, if the surface dangling bonds of Si grains are passivated by H atoms and if they are present in interstellar space in quantities sufficient to account for the observed ERE, we would expect to see the Si-H 15.6 $\mu$ m wagging, 11.6 $\mu$ m bending, and even 5 $\mu$ m stretching bands (Adachi 1999).

We especially thank A.N. Witt for invaluable comments and helpful suggestions, and L. Verstraete for providing us with the ISO spectrum of NGC 2023 in advance of publication. We also thank S. Adachi, N. Koshida, P. Maddalena, and V.G. Zubko for sending us their optical constants of bulk Si and/or nano-silicon; S. Adachi, L.J. Allamandola, J.M. Greenberg, Th. Henning, N. Koshida, D. Kovalev, P. Maddalena, L. Pavesi, and K. Sellgren for helpful suggestions; and R.H. Lupton for the availability of the SM plotting package. This research was supported in part by NASA grant NAG5-7030 and NSF grants AST-9619429 and AST-9988126.

## REFERENCES

- Adachi, S. 1999, *Optical Constants of Crystalline and Amorphous Semiconductors – Numerical Data and Graphical Information* (Dordrecht: Kluwer)
- Arendt, R.G., et al. 1998, *ApJ*, 508, 74
- Ashcroft, N.W., & Mermin, N.D. 1976, *Solid State Physics* (New York: Holt, Rinehart, & Winston)
- Bohren, C.F., & Huffman, D.R. 1983, *Absorption and Scattering of Light by Small Particles* (New York: Wiley)
- Cardelli, J.A., Clayton, G.C., & Mathis, J.S. 1989, *ApJ*, 345, 245

- Darbon, S., Perrin, J.-M., & Sivan, J.-P. 1999, *A&A*, 348, 990
- Darbon, S., Zavagno, A., Perrin, J.-M., Savine, C., Ducci, V., & Sivan, J.-P. 2000, *A&A*, 364, 723
- Diesinger, H., Bsiesy, A., & Hérino, R. 2001, *J. Appl. Phys.*, 89, 221
- Draine, B.T., & Bertoldi, F. 1996, *ApJ*, 468, 269
- Draine, B.T., & Bertoldi, F. 2000, in *H<sub>2</sub> in Space*, ed. F. Combes, & G. Pineau des Forêts (Cambridge: Cambridge University Press), 131
- Draine, B.T., & Li, A. 2001, *ApJ*, 551, 807
- Duley, W.W. 1985, *MNRAS*, 215, 259
- de Filippo, F., de Lisio, C., Maddalena, P., Léron del, G., & Altucci, C. 2000, *Phys. Stat. Sol. A*, 182, 261
- Gordon, K.D., Witt, A.N., & Friedmann, B.C. 1998, *ApJ*, 498, 522
- Gordon, K.D., et al. 2000, *ApJ*, 544, 859
- Gray, D.E. 1972, *American Institute of Physics Handbook* (McGraw-Hill Book Company)
- Greenberg, J.M. 1968, in *Stars and Stellar Systems*, Vol. VII, ed. B.M. Middlehurst & L.H. Aller (Chicago: Univ. of Chicago Press), 221
- Habing, H.J. 1968, *Bull. Astron. Inst. Netherlands*, 19, 421
- Harrington, J.A., Rudisill, J.E., & Braunstein, M. 1978, *Appl. Opt.*, 17, 1541
- Harvey, P.M., Thronson, H.A., Jr., & Gatley, I. 1980, *ApJ*, 235, 89
- d'Hendecourt, L.B., Léger, A., Olofson, G., & Schmidt, W. 1986, *A&A*, 170, 91
- Henning, Th., & Mutschke, H. 1998, *A&A*, 327, 743
- Hofmeister, A.M., Rosen, L.J., & Speck, A.K. 2000, in *Thermal Emission Spectroscopy and Analysis of Dust, Disks, and Regoliths*, ed. M.L. Sitko, A.L. Sprague, & D.K. Lynch, *ASP Conf. Series*, 196, 291
- Johnson, F.A. 1959, *Proc. Phys. Soc. London*, 73, 265
- Koshida, N., et al. 1993, *Appl. Phys. Lett.*, 63, 2774
- Kovalev, D., Polisski, G., Ben-Chorin, M., Diener, J., & Koch, F. 1996, *J. Appl. Phys.*, 80, 5978
- Kovalev, D., Heckler, H., Polisski, & Koch, F. 1999, *Phys. Stat. Sol. B*, 215, 871
- Ledoux, G., et al. 1998, *A&A*, 333, L39
- Ledoux, G., Guillois, O., Porterat, D., Reynaud, C., Huisken, F., Kohn, B., & Paillard, V. 2000, *Phys. Rev. B*, 62, 15942
- Léron del, G., Madéore, F., Romestain, R., & Muller, F. 2000, *Thin Solid Films*, 366, 216
- Li, A., & Draine, B.T. 2001, *ApJ*, 553, 000 (astro-ph/0011319)
- Mathis, J.S., Mezger, P.G., & Panagia, N. 1983, *A&A*, 128, 212

- McCartney, M.S.K., Brand, P.W.J.L., Burton, M.G., & Chrysostomou, A. 1999, MNRAS, 307, 315
- Ossenkopf, V., Henning, Th., & Mathis, J.S. 1992, A&A, 261, 567
- Palik, E.D. 1991, Handbook of Optical Constants of Solids (Boston: Academic)
- Papoular, R., Conard, J., Guillois, O., Nenner, I., Reynaud, C., & Rouzaud, J.-N. 1996, A&A, 315, 222
- Perrin, J.-M., & Sivan, J.-P. 1992, A&A, 255, 271
- Sakata, A., Wada, S., Narisawa, T., Asano, Y., Iijima, Y., Onaka, T., & Tokunaga, A.T. 1992, ApJ, 393, L83
- Schmidt, G.D., Cohen, M., & Margon, B. 1980, ApJ, 239, L133
- Seahra, S.S., & Duley, W.W. 1999, ApJ, 520, 719
- Sivan, J.-P., & Perrin, J.-M. 1993, ApJ, 404, 258
- Smith, T.L., & Witt, A.N. 2001, in preparation
- Snow, T.P., & Witt, A.N. 1996, ApJ, 468, L65
- Szomoru, A., & Guhathakurta, P. 1998, ApJ, 494, L93
- Theiss, W. 1997, Surf. Sci. Rep., 29, 91
- Tsu, R., Babic, D., & Ioriatti, L., Jr. 1997, J. Appl. Phys., 82, 1327
- Uchida, K.I., Sellgren, K., & Werner, M.W. 1998, ApJ, 493, L109
- Verstraete, L., et al. 2001, A&A, in press
- Wang, L.W., & Zunger, A. 1994, Phys. Rev. Lett., 73, 1039
- Webster, A. 1993, MNRAS, 264, L1
- Weingartner, J.C., & Draine, B.T. 2001, ApJ, 548, 296
- Wilson, W.L., Szajowski, P.F., & Brus, L.E. 1993, Science, 262, 1242
- Witt, A.N., & Boroson, T.A. 1990, ApJ, 355, 182
- Witt, A.N., Gordon, K.D., & Furton, D.G. 1998, ApJ, 501, L111
- Witt, A.N., & Schild, R. 1988, ApJ, 325, 837
- Witt, A.N., Schild, R.E., & Kraiman, J.B. 1984, ApJ, 281, 708
- Yoffe, A.D. 2001, Adv. Phys., 50, 1
- Zubko, V.G., Smith, T.L., & Witt, A.N. 1999, ApJ, 511, L57